

VERIFICATION OF EUROCODE DESIGN MODELS ON THE CALCULATION OF STRENGTHS AND DEFLECTIONS IN COLD- FORMED STEEL BEAMS

Jun Ye*, **Seyed Mohammad Mojtabaei****, **Iman Hajirasouliha****, **Paul Shepherd*** and
Kypros Pilakoutas**

*Department of Architecture and Civil Engineering, University of Bath, Bath, BA2 7AY, UK
j.ye@bath.ac.uk

**Department of Civil Engineering and Structural Engineering, The University of Sheffield, Sheffield, S1 3JD,
UK

Keywords: Cold-formed Steel; Beam; Finite Element Study; Strength; Deflection.

Abstract. *This paper develops a numerical model to investigate the flexural strength and failure modes of CFS back-to-back channel beams and verifies the efficiency of an optimisation framework previously proposed. The model incorporates non-linear stress-strain behaviour and enhanced corner properties obtained from coupon tests, as well as initial geometric imperfections measured in physical specimens. To simulate the behaviour of a bolt bearing against a steel plate in the back-to-back section, a connector model is used that takes into account both slippage and bearing deformations. The developed Finite Element (FE) models are verified against six four-point bending tests on CFS back-to-back channel beams, where excellent agreement is found between the experimental results and the FE predictions. The validated FE models are then used to assess the adequacy of the effective width method in EC3 and the Direct Strength Method (DSM) in estimating the design capacity of conventional and optimum design CFS channel beam sections. The results indicate that both EC3 and DSM provide accurate predictions for the bending capacity of lipped channel beam sections. A comparison between FE predictions and tested results show that, on average, the geometric imperfections can change the FE predictions of ultimate capacity by up to 11%, while the strain-hardening of CFS material at the round corners has negligible effects. It is also shown that EC3 uses a reduced cross-sectional property to calculate deflections, which can reasonably predict deflections with a slight overestimation (6%) at the serviceability load level.*

1 INTRODUCTION

Cold-formed steel (CFS) members have traditionally been employed as load-carrying members in a wide range of applications, such as roof purlins and structural envelopes. In recent years, however, CFS members have become increasingly popular in low- to mid-rise multi-storey buildings [1] and CFS portal frames with short to intermediate spans [2, 3]. CFS sections are increasingly being offered as an alternative to hot-rolled steel elements since they provide greater flexibility in terms of cross-sectional profiles and sizes, which can lead to more efficient design solutions with less redundant material. CFS sections are also lightweight, easy to handle on site, and easier to connect. However, CFS components are made of thin plates, which have inherently low buckling resistance. This results in reduced strength for CFS elements, which limits their performance in multi-storey applications. CFS components are usually susceptible to local, distortional and global buckling (and their interactions).

Although the accurate prediction of the behaviour of CFS elements is difficult due to their complex failure modes, Finite Element Analysis (FEA) is widely used to predict the flexural behaviour of CFS beams [4]. Compared to physical experiments, FEA is relatively inexpensive and time efficient, especially when a parametric study of cross-section geometry

is involved. In addition, FEA can be efficiently used for investigations considering geometric imperfections and material nonlinearity of structural members, which could be difficult to achieve through physical tests.

This paper aims to develop an advanced numerical model to predict the flexural behaviour and bending strength of CFS beam sections CFS back-to-back channel beams and to verify an optimisation framework previously proposed. An experimental investigation, including six physical tests on CFS back-to-back channel beams, which failed by local/distortional buckling about the major axis, is used to verify the FE models in ABAQUS [5]. The advantage of the developed models over the previous studies is that it incorporates non-linear stress-strain behaviour and enhanced material properties based on coupon tests, measured initial imperfections and an effective connector element to model the bolt behaviour. The models are then used to assess the adequacy of both the EC3 design guides [6-8] and the Direct Strength Method (DSM) to design a range of conventional and optimum designed CFS beams considering local/distortional buckling modes. The deflection of CFS beams incorporating the effects of the material non-linearity, effective cross-sections and the change of Young's modulus along the distribution of bending moment in the beams, is also investigated.

2 OPTIMISATION OF CFS BEAMS

In this section an optimisation framework proposed by the authors [9, 10] is adopted for optimum design of a back-to-back channel section by taking into account the interaction between local and distortional buckling modes. The objective function is to obtain a design solution with maximum bending capacity but within the deflection criteria as follows:

$$\max M_{c,Rd} = \chi_{LT} \cdot W_{eff} \cdot f_y \quad (1)$$

subject to:

$$b/t \leq 60, c/t \leq 50, h/t \leq 500 \quad (2)$$

$$0.2 \leq c/b \leq 0.6 \quad (3)$$

$$b \geq 50, c \leq 25 \quad (4)$$

$$\Delta < \Delta_{lim} \quad (5)$$

where h is the cross-sectional height, and b and c are the flange and lip width, respectively. W_{eff} is the effective modulus of the cross-section considering the local/distortional buckling. χ_{LT} is the reduction factor taken into account the lateral-torsional buckling. f_y is the yield stress of the material used. Eqs.(2) and (3) represent the width-to-thickness ratio limits defined in EC3, Part 1.3 [7]. Eq.(4) is used to take into account the manufacturing and construction constraints.

Eq.(5) imposes a constraint on the upper limit of deflection $\Delta_{lim}=L/200$ ($L=1200$ mm is the beam span) of the CFS beams [11]. A load factor of $1/1.35=0.74$ is used when calculating the deflections using effective cross-section according to EC3, Part 1.5 and Part 1.3 [6, 7], which means the deflection is obtained by using a moment ratio of $M_s = 0.74M_{c,Rd}$. This is due to the fact that in the ultimate limit state design of CFS beams, the partial factor of 1.35 is used for the dead load while 1.5 is used for the live load. However, these partial factors are 1.0 for serviceability limit state design. A load factor of $1/1.35=0.74$ means a slightly larger deflection will be calculated which can be in the safe side. When calculating the deflection, a uniform bending moment is applied at both ends of a simply-supported beam.

Fig.1 shows the nominal dimensions of the three different cross-sections used in this study. All the dimensions in this figure are in *mm* and are defined between the outer to outer surfaces. The cross-section A230 is a standard commercially available cross-section, while section B270 is the optimum solution with the highest flexural strength subject to the constraints in Eqs.(2) to (5). Cross-section C180 is a benchmark section (with a flange width between the flange widths of sections A230 and B270) used for comparison purposes. All cross-sections have the same nominal thickness $t = 1.5\text{mm}$ and coil width of steel sheet $l = 415\text{mm}$ to use the same amount of material. The values for the radius of the round corner, the elastic modulus and the Poisson's ratio used were taken as 3mm , 210GPa and 0.3 , respectively. The yield stress of the CFS material was considered to be $f_y = 450\text{MPa}$ in the optimisation process.

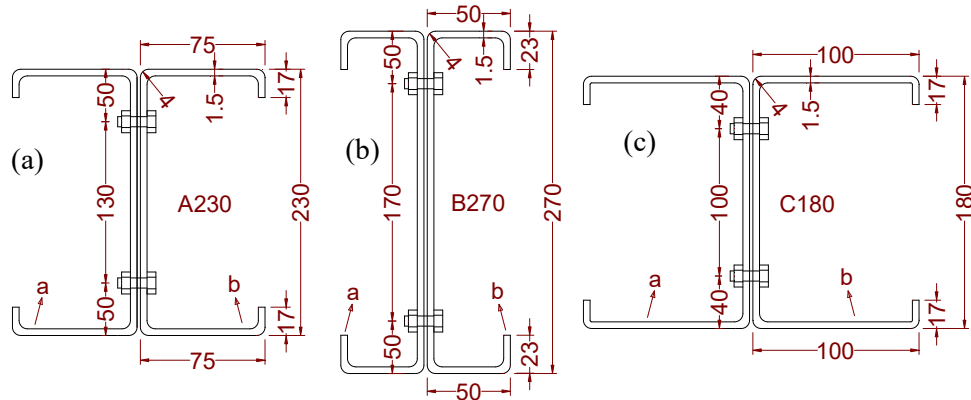


Figure 1: Symbol definitions and nominal cross-sectional dimensions: (a) A230; (b) B270 and (c) C180

The three sections were manufactured using the press breaking process and were tested about their major axis using a four-point bending set-up as shown in Fig.2 to obtain their flexural strength. For each cross-section, two similar specimens with the same cross-section were tested to ensure the consistency of the results. The non-linear stress-strain behaviour and enhanced corner properties of the material were obtained based on the results of six tensile coupons. Tensile coupons were extracted from both the flat and the corner regions of the cross-sections to determine the material properties. The geometric imperfections of the back-to-back specimens were recorded using a specially designed measurement rig. More information about the conducted experimental tests can be found in [12].

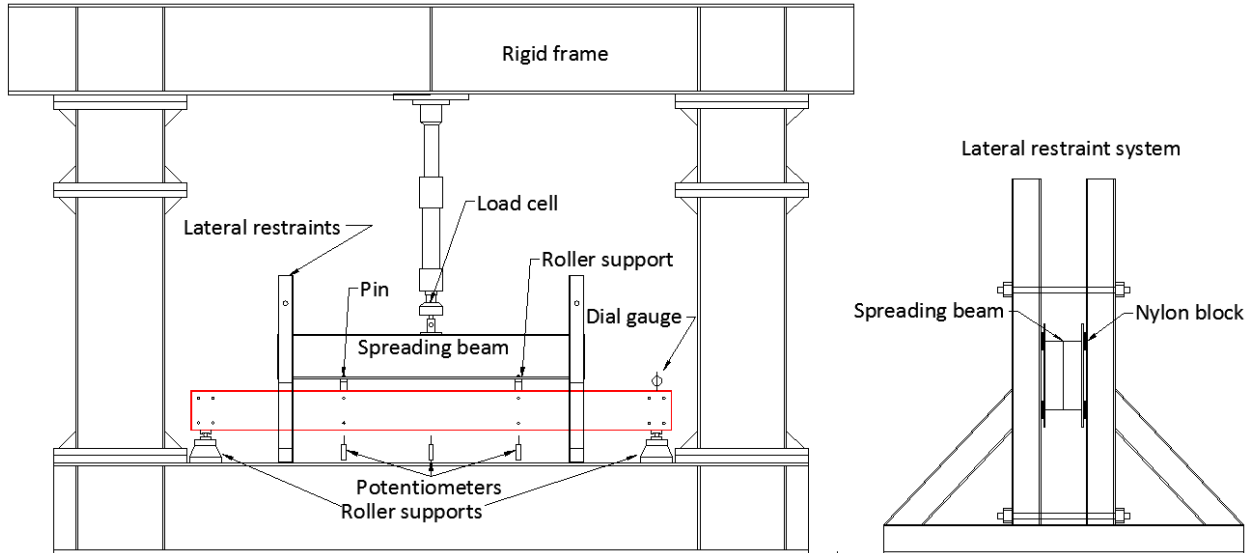


Figure 2: Typical experimental set-up of four-point bending tests of back-to-back beam sections

3 NUMERICAL MODELLING

3.1 Material model

The inelastic properties of CFS material were found to have significant effects on the ultimate capacity and post-buckling behaviour of CFS beams [13]. In this study, the results of the six tensile coupon tests from the flat plates and round corner regions of the cross-sections were used to investigate the effects of the forming process on the material properties. The material model was then included in the FEM by using the true stress vs true strain curve, which was calculated from the following equations:

$$\sigma_{true} = \sigma(1 + \varepsilon) \quad (6)$$

$$\varepsilon_{true} = \ln(1 + \varepsilon) \quad (7)$$

where σ and ε are the measured engineering stress and strain, respectively, based on the original cross-section area of the coupon specimens. The resulting stress-strain curves for both the flat plates and round corner areas (Fig.3) were also incorporated into ABAQUS[5].

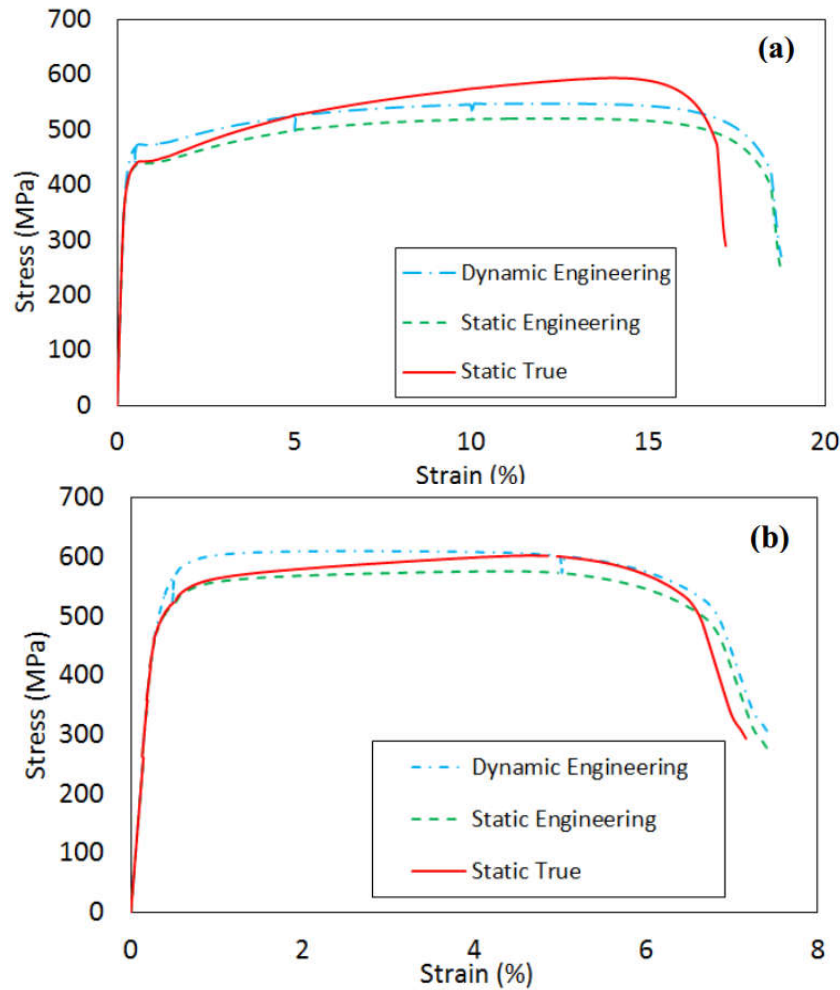


Figure 3: Stress–strain curves resulted from (a) flat and (b) corner coupon tests

3.2 Boundary conditions

The CFS back-to-back beams were tested in a four-point bending configuration, as illustrated in Fig.2. The specimens were supported on rollers located 3100 mm apart. All specimens were bent about their major axis. The load was applied through a spreader beam onto the test specimens at two discrete locations 1200 mm apart. The spreader beam was restrained against any out-of-plane movement by a specially designed guidance system, as shown in Fig.2. Nylon blocks were used as bearing pads between the spreader beam and the uprights in order to reduce vertical friction. A pin and a roller support were used to transfer the load from the spreader beam to the specimen. These supports were also designed to restrain any out-of-plane displacement of the top flange of the test specimen. To simulate the boundary conditions of the experimental program, a simply supported condition was used at both ends of the FE models as shown in Fig.4. Two reference points were established at the positions of the roller and pin supports at the middle of the gap between the top two flanges of the CFS back-to-back beams to apply the external loads. The nodes under the region of the supports were coupled to the related reference point corresponding to the pin and roller supports as indicated in Fig.4.

In order to avoid the localised bearing failure of the CFS sections during the experimental tests, wooden blocks were packed into the cross-section at the loading points and the end

supports. Therefore, in the FE models, the elastic modulus of $10E$ was used for the steel plates in the areas with the wood blocks to simulate the rigid behaviour. A rigid body constraint, with a reference point at the middle of the gap between the two bottom flanges of the CFS back-to-back beams, was used at both ends of the CFS beam to prevent localised failure at the supports. To simulate the roller supports at the two ends of the CFS beams, the translational and rotational degrees of freedoms at the reference points were set to be $U_2=UR_3=0$ (see Fig.3). Regarding the reference points at the loading positions, the translations of U_1 and U_3 were fixed at the pin support while $U_1=0$ was used at the roller support. This was to prevent the lateral deformation and longitudinal displacement of the CFS beams at these locations.

The CFS back-to-back beams were assembled by using two single channels with bolts as shown in Fig. 1. A connector element was used to model the bolt behaviour as will be explained in Section 3.4. Contact pairs were also defined between the two webs of each CFS single channel section using a surface-to-surface contact property. In the normal direction of the contact pairs, a “hard” surface was used while in the tangent direction between the two profiles a “frictionless” property was defined.

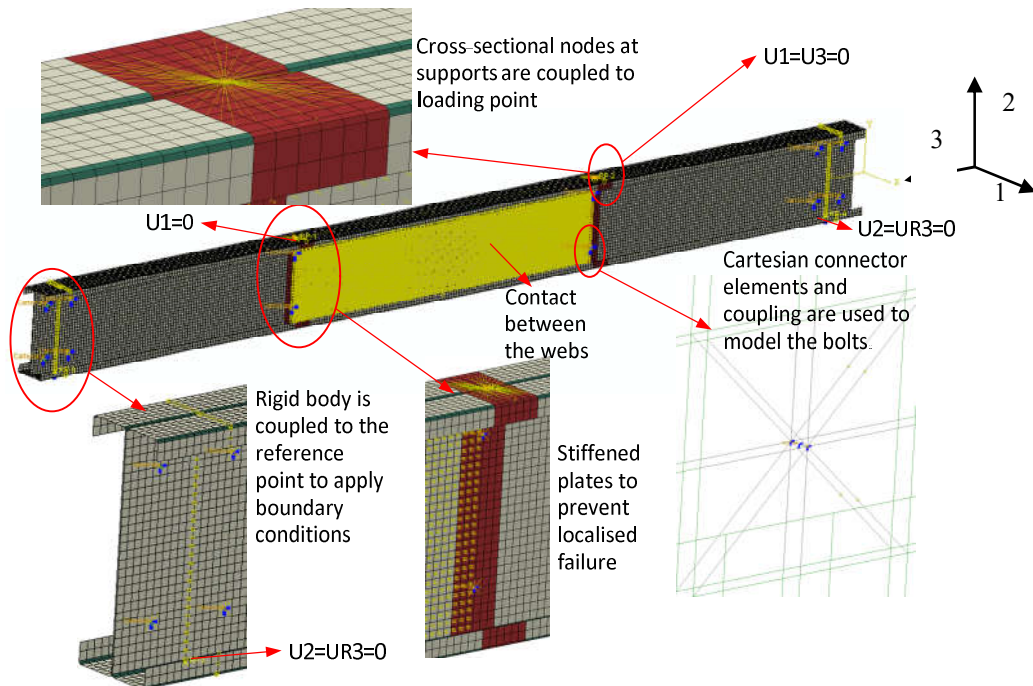


Figure 4: Boundary conditions of FE model against test

3.3 Element type and mesh size

A four-node, quadrilateral shell element (S4R) with reduced integration and hourglass control was used for the modelling of the CFS beams. This shell element can take into account transverse shear deformations and has been successfully used in the modelling of CFS beam sections by other researchers [14-16].

The effects of mesh size in the FE model on the behaviour of the CFS beams were firstly investigated. It was found that using a 10x10mm element dimension for the CFS channels provides a balance between computational time and accuracy. Therefore, 10x10mm elements

were used for all FE simulations in this study. However, for the modelling of the corners of the CFS sections, it was found that two elements were suitable for the modelling of each round corner.

3.4 Modelling of bolts

It was found from reference experimental tests [17-19] that the position and behaviour of bolts can considerably influence the moment-rotation behaviour of the back-to-back CFS beams. The failure mode of the tested beams was also demonstrated to be significantly affected by the bolt slippage and bearing deformation. Therefore, it is important to develop an appropriate model in ABAQUS to simulate the local load-deformation behaviour of a single bolt bearing against a single steel sheet. Lim and Nethercot [2, 3] used a simplified bolt model which consisted of two perpendicular nonlinear springs to model the bearing behaviour of a single bolt. In their study, good agreement was achieved between experimental test results and the modelled behaviour of CFS full-scale joints subjected to monotonic load. A more direct method to model bolt behaviour using FE analysis is to use solid brick element and surface-to-surface contact interactions in ABAQUS [20-22]. The disadvantage of this model is that using solid elements makes the model more complex and, therefore, reduces the computational efficiency, especially in models with a large number of bolts. In addition, due to the presence of bolt rigid body movement and slippage, convergence could also be an issue [22]. A practical technique is therefore presented here to simulate the slippage and bearing behaviour of the bolts in CFS back-to-back sections.

For CFS back-to-back channels assembling, a fastener tension (preloading force) is applied to the head of the bolt by using a torque wrench. The torque-preloading relationship is often simplified by using a constant K , known as the torque coefficient, as shown in the following equation [23, 24]:

$$T = K \cdot P_b \cdot d \quad (8)$$

where T ($N\cdot mm$) is the input tightening torque applied to the fastener head or nut, P_b (N) is the preloading force and d (mm) is the nominal bolt diameter. An approximate value of 0.2 has been used for the torque coefficient [23, 24]. This results in an equivalent preloading force of $P_b = 6.25kN$, which is close to the results presented by Croccolo *et al.* [25]. The slippage behaviour of the bolts depends mainly on the distribution of initial friction forces, which in return relies on the bolt pretension force P_b for a given applied torque and friction coefficient μ of the contact surfaces. The following formula is used to calculate the bolt slip resistance F_{slip} [26]:

$$F_{slip} = \mu \cdot P_b \cdot n_b \quad (9)$$

where μ is the mean frictional coefficient taken as 0.19 for galvanised steel surfaces [26], and n_b is the number of slip planes.

A single bolt can transfer shear forces to a CFS member through the bearing behaviour in addition to slippage described above. Once the slippage deformation overcomes the gap between the bolt shank and the steel sheet, the bearing behaviour of the bolt against steel sheet will be activated. Fisher [27] proposed the following equation to take into account the bolt bearing force and the bearing deformation relationship:

$$R_B = R_{ult} \left[1 - e^{-\mu(\delta_n/25.4)} \right]^\lambda \quad (10)$$

$$R_{ult} = 2.1 \cdot d \cdot t \cdot F_u \quad (11)$$

where δ_{br} is the bearing deformation (mm), R_{ult} is the ultimate bearing strength, t is the web thickness, d is the bolt diameter and R_B is the bearing force against the bearing deformation. F_u is the tensile strength of the web plate material, which can be obtained from coupon tests. $e = 2.718$ is the nature exponential, while $\mu = 5$ and $\lambda = 0.55$ are the regression coefficients presented by Uang *et al.* [28].

In the reference experimental tests [12], the bolt shank diameter was 12mm. The bolt slippage behaviour is generally defined for a limited range of slip movement within the bolt hole clearance (typically ± 1 mm for standard bolts by assuming that the bolt shanks are centrally positioned). According to Eqs.(8)-(11), a slip-bearing relationship can be defined as shown in Fig. 5.

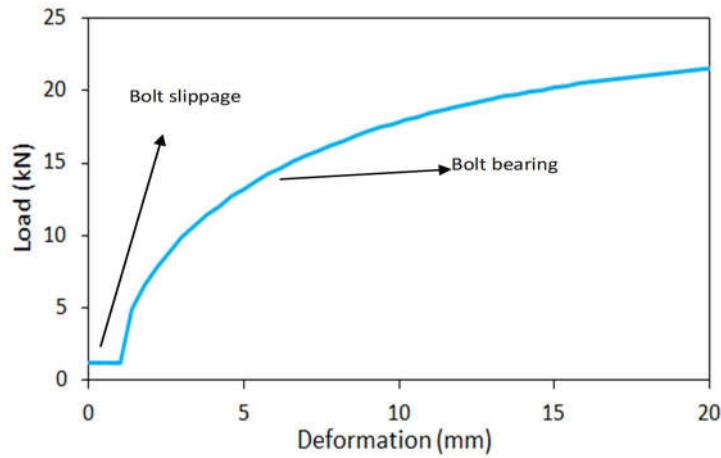


Figure 5: Load-deformation relationship of a bolt slipping and bearing against a steel plate

In order to model a group of bolts, the connector element in ABAQUS [5] was used, as shown in Fig.6 (a). For each single bolt in Fig.6 (a), a two-layer fastener configuration was used at the position of each individual bolt in the full-scale connection (see Fig.6 (b)). The layer was connected by a node in one channel section and a point in its counterpart section using a connector element to define the bolt property. The connector type of “Cartesian” with 3 translational degrees of freedom at each node was employed. This connector was characterised by a parallel combination of “Elasticity” and “Plasticity” behaviours, as defined in ABAQUS [5]. In the “Elasticity” behaviour, the rigid definition was used in the corresponding shear direction. For the definition of “Plasticity” behaviour, the load-deformation relationship shown in Fig.5 was employed to represent the behaviour of a bolt which is slipping and bearing against a steel plate. It should be noted that the “Elasticity” and “Plasticity” behaviours are defined in local coordinate systems corresponding to the shear deformation of the bolts.

The bolt slippage and bearing behaviour, which are defined in Eqs. (8)-(11), are included in the connector element shown in Fig.6(a). Therefore, it is important to exclude the bearing deformation stemmed from the bearing of each node at the bolt position. To achieve this, constraints “Coupling” in ABAQUS [5] was employed, and its definition is shown in Fig.6(b). Each node at the position of the bolts was thereby connected to the nearby nodes in the CFS steel plates using the constraint that couples the displacement and rotation. These nodes should lie in a reasonably large region in the plates to reduce the bearing deformation.

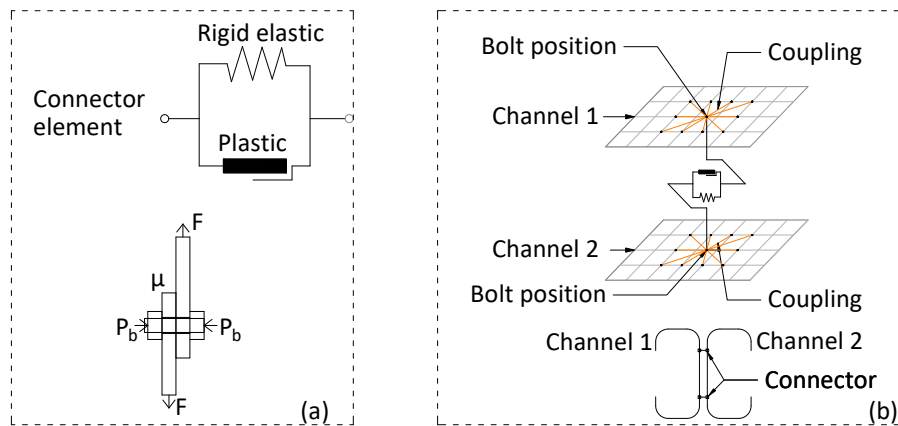


Figure 6: Single bolt modelling in ABAQUS: (a) components defined in a connector; (b) reducing the bearing behaviour by coupling the node at the bolt position to a number of nodes close-by

3.5 Imperfections

The stability of thin-walled CFS members may in some cases be significantly affected by the presence of imperfections, especially when interactive buckling of different modes is involved. In the reference experimental programme, the magnitude and the shape of the geometric imperfections of each specimen were therefore recorded before testing. The imperfections were measured along the five longitudinal lines indicated in Fig. 7, by means of reflected laser beams. As a first step, the raw data were decomposed into its respective Fourier series and a finite number of terms were removed to cut off the high frequency vibrations originating from the driving mechanisms of the moving motors. Using this reduced Fourier series resulted in a more continuum node coordinates adjustment when the measured imperfections were included. Within a given cross-section, the magnitude of the imperfection at each node of the FE mesh was determined by interpolation of the measurements. Quadratic interpolation was used for the web imperfections, while linear interpolation was used at the flanges. The coordinates of each node in the FE models were then adjusted to account for the imperfections.

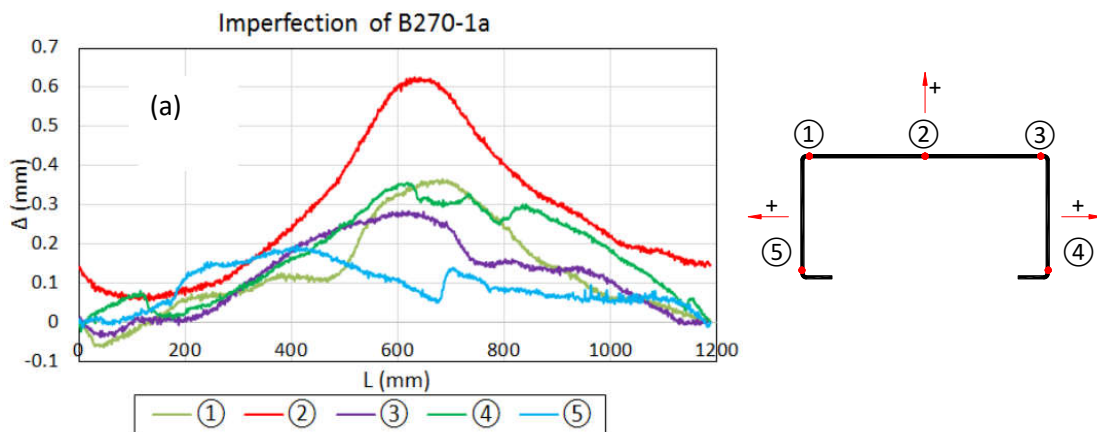


Figure 7: Measured imperfection of B270-1a

3.6 Numerical results

Table 1 compares the ultimate load carrying capacities M_u resulting from the FE models against those obtained from the reference experiments on the CFS lipped channel beams with different cross-sections. M_{u1} is the predicted flexural strength that takes into account the strain hardening effect of the material in the corner region but without incorporating the geometric imperfections. M_{u2} indicates the predicted moment capacity where only the effect of the measured initial geometric imperfections was taken into account. The predicted capacity M_{u3} , on the other hand, considers both the measured initial geometric imperfections and the strain hardening effect of the material in the corner regions.

Table 1: Comparison of FE results with tested flexural strength

Specimen	M_u (kN·m)	M_{u1} (kN·m)	M_{u2} (kN·m)	M_{u3} (kN·m)	M_{u1} / M_u	M_{u2} / M_u	M_{u3} / M_u
A230-1	23.72	25.31	23.12	23.94	1.067	0.975	1.009
A230-2	23.79	25.58	22.39	23.92	1.075	0.941	1.005
B270-1	(25.83)	28.87	25.95	26.11	--	--	
B270-2	28.34	28.25	27.82	28.47	0.997	0.982	1.005
C180-1	17.43	18.22	16.41	17.68	1.045	0.941	1.014
C180-2	17.24	17.89	16.53	17.55	1.038	0.959	1.018
Average					1.044	0.960	1.010
St. Dev.					0.031	0.019	0.006

As shown in Table 1, excellent agreement was obtained between experimental results and FE predictions. The average ratio of the FE predicted bending capacity M_{u2} to the experimentally measured flexural strength M_u was 0.960, with a standard deviation of 0.019. In comparison, the average ratio of the FE predicted bending capacity M_{u3} to the experimentally measured load carrying capacity M_u was 1.010, with a standard deviation of 0.006. This indicates that considering the strength variation caused by the strain hardening effect of the round corner material in the current test series could increase the accuracy of the bending capacity predictions by 5%, which is not significant. However, by comparing the predicted flexural strength M_{u1} with M_{u3} , it is shown that the initial geometric imperfections can have considerable effects on the load carrying capacity (up to 11%). It should be noted that, on average, the variation of flexural strength is 3.1% and 0.6%, with and without taking into account the geometric imperfections, respectively.

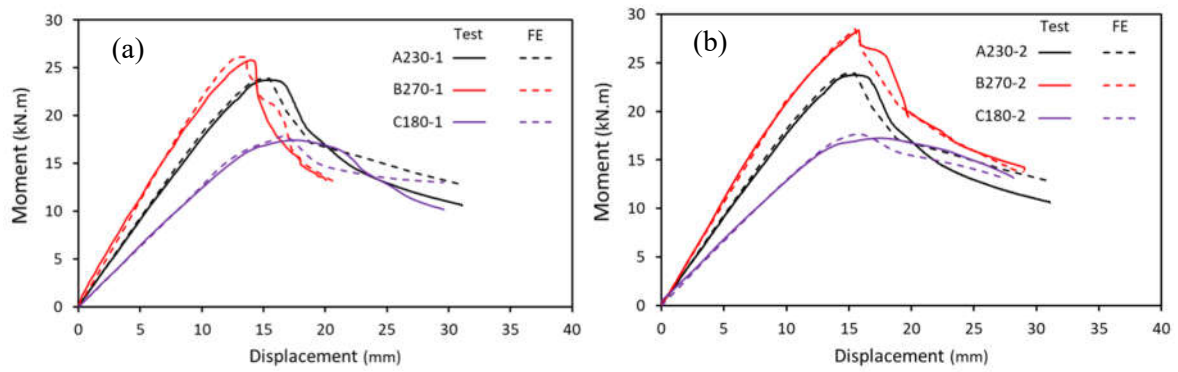


Figure 8: Moment versus mid-span deflection relationship resulting from FE against Test: (a) specimens A230-1, B270-1 and C180-1; (b) specimens A230-2, B270-2 and C180-2

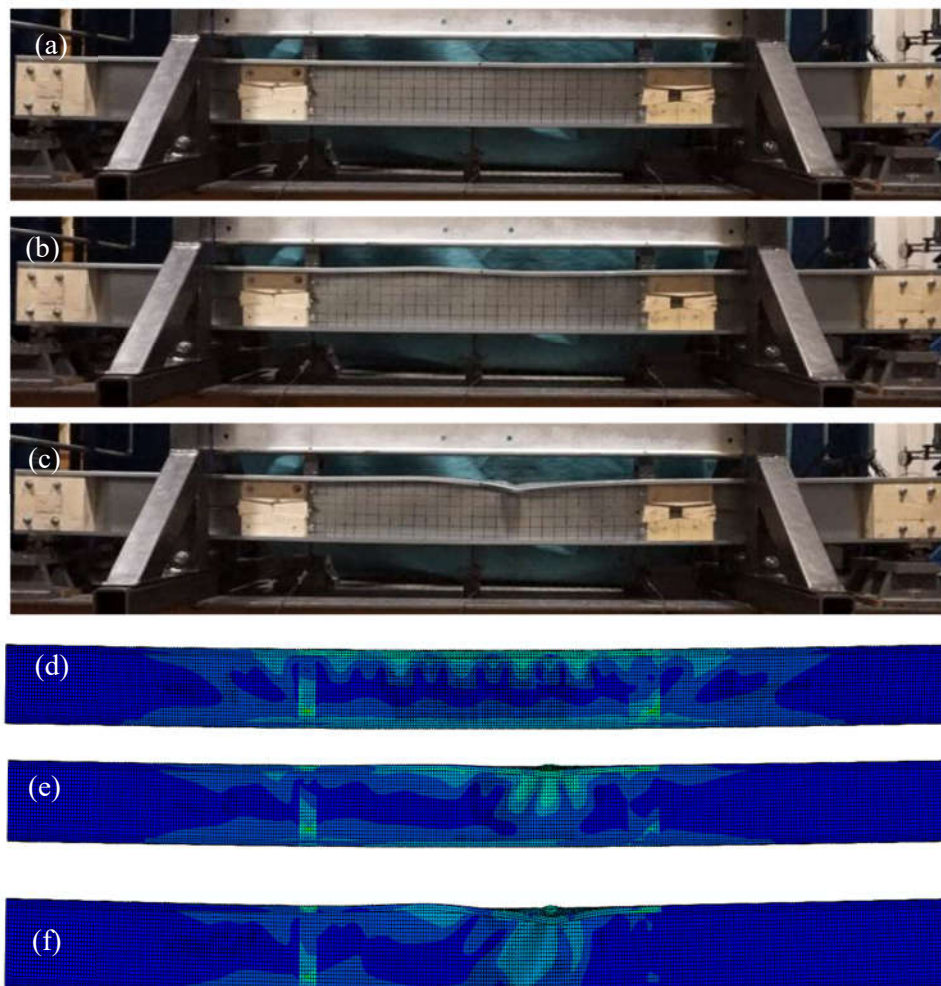


Figure 9: Deformation of FE model vs actual specimen A230-2: (a-c) tested deformations and (d-f) numerical modelling deformations

Fig.8 illustrates the tested moment versus mid-span deflection curves corresponding to the reference experimental tests and the predicted results from numerical study. It is shown that the proposed FE model was able to capture the peak load and stiffness of CFS beam sections with a very good accuracy. Fig 9 compares the failure shape of the tested specimen A230-2

with the predicted deformation of the corresponding FE models. It is shown that the proposed FE model could also predict well the failure modes of the CFS beams. These results confirm the adequacy of the developed FE models in simulating the actual behaviour of CFS back-to-back beam channels up to their failure points.

4 EVALUATION OF CURRENT DESIGN METHODS

In this section, the experimental results are compared to the predictions of the Direct Strength Method (DSM) and EC3 design methods. The specimen B270-1 was tested without the wood blocks and was failed by a localised failure at the top flange rather than the expected bending failure. Therefore, the result of specimen B270-1 was not considered here. As shown in Table 2, both DSM and EC3 predictions on the bending capacity of CFS back-to-back beams were accurate enough for practical design considerations. The ratio of the DSM predicted load capacity to the experimentally measured load carrying capacity was 0.96, with a standard deviation of 0.05. It is evident from Table 2 that the “effective width” based method comprised in EC3 generally leads to accurate predictions (on average 99% with a standard deviation of 9%) of the beam strengths. However, the EC3 results in some cases can be up to 10% overestimated.

Table 2: Evaluation of the DSM and EC3 design methods to predict the bending capacity

Specimen	Test (<i>kN·m</i>)	EC 3 (<i>kN·m</i>)	DSM (<i>kN·m</i>)	EC3 / Test	DSM/Test
A230-1	23.72	22.38	22.42	0.94	0.95
A230-2	23.79	22.59	22.61	0.95	0.95
B270-1	(25.83)	25.26	25.76	--	--
B270-2	28.34	25.09	25.38	0.89	0.90
C180-1	17.43	18.77	17.42	1.08	0.99
C180-2	17.24	18.91	17.40	1.10	1.01
Average				0.99	0.96
St. Dev.				0.09	0.05

5 DETERMINE DEFLECTIONS OF CFS BACK-TO-BACK BEAMS

Serviceability criteria should be also taken into account in CFS beam design, especially for supporting beams in long span roof or floor systems. Eurocode 3 Part 1-3 stipulates that the effective cross-section for the serviceability limit state should be used in all serviceability limit state calculations for CFS members. In determination of the cross-sectional properties of CFS sections, the effective parts of individual plates in the cross-section will be different according to the stress levels obtained from the distribution of bending moments. Meanwhile, the deflections are generally estimated by using the secant modulus of elasticity, especially in alloys with pronounced strain hardening behaviour.

To predict the deflections of the tested beams, six different cases (including the method suggested by EC3) were considered by varying the material nonlinearity (using the secant modulus of elasticity) and moment gradient along the beam span. The results were then compared with those obtained from the reference experimental tests. This will help to assess the errors associated with any of these simplifying assumptions and identify the best practical method to calculate the deflection of CFS beams:

Method 1: Calculation of deflections using a constant modulus of elasticity (E_{s0}) at the initial stage of the nonlinear stress-strain curve, and gross cross-section properties (I) along the length of the beam.

$$d = \int_0^{L_1} \frac{M(x) \cdot x}{E_{s0} \cdot I} dx \quad (12)$$

where d is the calculated deflection, $M(x)$ is the bending moment at the position of x and L_1 is the beam span to be considered.

Method 2: Assuming constant modulus of elasticity (E_{s0}) at the initial stage of the nonlinear stress-strain curve to calculate the deflections, but with the effective cross-sectional property $I_{eff,max}$ determined at the maximum stress level along the beam span:

$$P \rightarrow M_{max} \rightarrow \sigma_{gr,max} \rightarrow b_{eff} \rightarrow I_{eff,max} \rightarrow d = \int_0^{L_1} \frac{M(x) \cdot x}{E_{s0} \cdot I_{eff,max}} dx \quad (13)$$

Method 3: Calculation of deflections using the constant modulus of elasticity (E_{s0}) at the initial stage of the nonlinear stress-strain curve but considering the variation of the effective cross-sectional properties $I_{eff}(x)$ at various stress levels along the length of the beams.

$$P \rightarrow M=M(x) \rightarrow \sigma(x) \rightarrow b_{eff}(x) \rightarrow I_{eff}(x) \rightarrow d = \int_0^{L_1} \frac{M(x) \cdot x}{E_{s0} \cdot I_{eff}(x)} dx \quad (14)$$

Method 4: Calculation of deflections considering variation of modulus of elasticity ($E_s(x)$) along the length of the beam, but using the constant gross cross-sectional property (I) of the beams.

$$P \rightarrow M=M(x) \rightarrow \sigma(x) = \frac{M(x)}{W} \rightarrow \varepsilon(x) \rightarrow E_s(x) \rightarrow d = \int_0^{L_1} \frac{M(x) \cdot x}{E_s(x) \cdot I} dx \quad (15)$$

Method 5: Calculation of the deflections considering the variation of modulus of elasticity ($E_s(x)$) along the length of the beam, and a change of effective cross-sectional property $I_{eff}(x)$ at various stress levels along the length of the beam:

$$P \rightarrow M=M(x) \rightarrow \sigma(x) = \frac{M(x)}{W} \rightarrow b_{eff}(x) \rightarrow \varepsilon(x) \rightarrow E_s(x) = \frac{\sigma(x)}{\varepsilon(x)} \rightarrow$$

$$d = \int_0^{L_1} \frac{M(x) \cdot x}{E_s(x) \cdot I_{eff}(x)} dx \quad (16)$$

Method 6: Calculation of the deflections using the Eurocode suggested methodology. The variation of the effective second moment of area I_{fic} is taken into account by using an interpolation between gross cross-sectional property I_{gr} and effective cross-section property

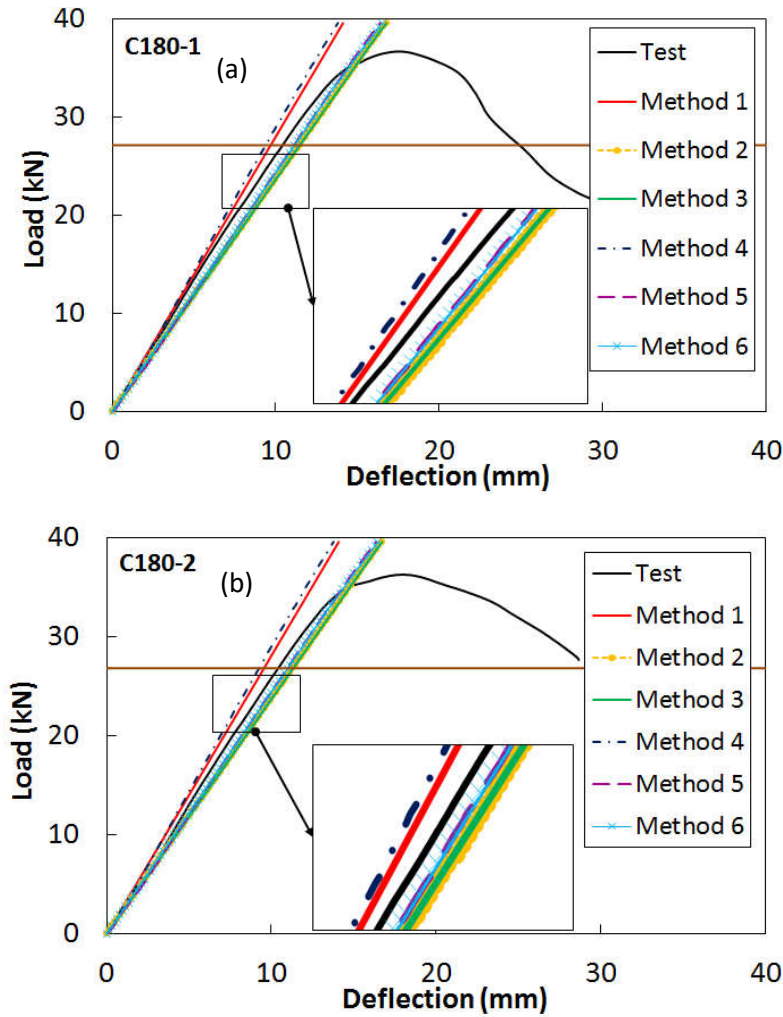
$I(\sigma_{eff,max})_{eff}$ determined at the maximum stress level $\sigma_{eff,max}$ using the effective cross-section along the beam:

$$I_{fic} = I_{gr} - \frac{\sigma_{gr}}{\sigma_{eff,max}} (I_{gr} - I(\sigma_{eff,max})_{eff}) \quad (17)$$

The calculation process is shown below using the constant modulus of elasticity (E_{s0}) at the initial stage of the nonlinear stress-strain curve:

$$\begin{aligned} P \rightarrow M \rightarrow \sigma_{gr} \rightarrow I_{gr} \rightarrow b_{eff} \rightarrow I_{eff} \rightarrow \sigma_{eff,max} \\ \rightarrow b_{eff}(\sigma_{eff,max}) \rightarrow I(\sigma_{eff,max})_{eff} \rightarrow I_{fic} \rightarrow d = \int_0^{L_1} \frac{M(x) \cdot x}{E_{s0} \cdot I_{fic}} dx \end{aligned} \quad (18)$$

The resulting deflections obtained for the tested beams, according to the methods presented in Eqs.(12)-(18) are analyzed. Fig.10 presents the resulting load-deflection curves at mid span compared to the load-deflection relationships recorded in the experiments. The horizontal line is the load level used for the design of the CFS beams at serviceability limit state, as presented in Section 2.



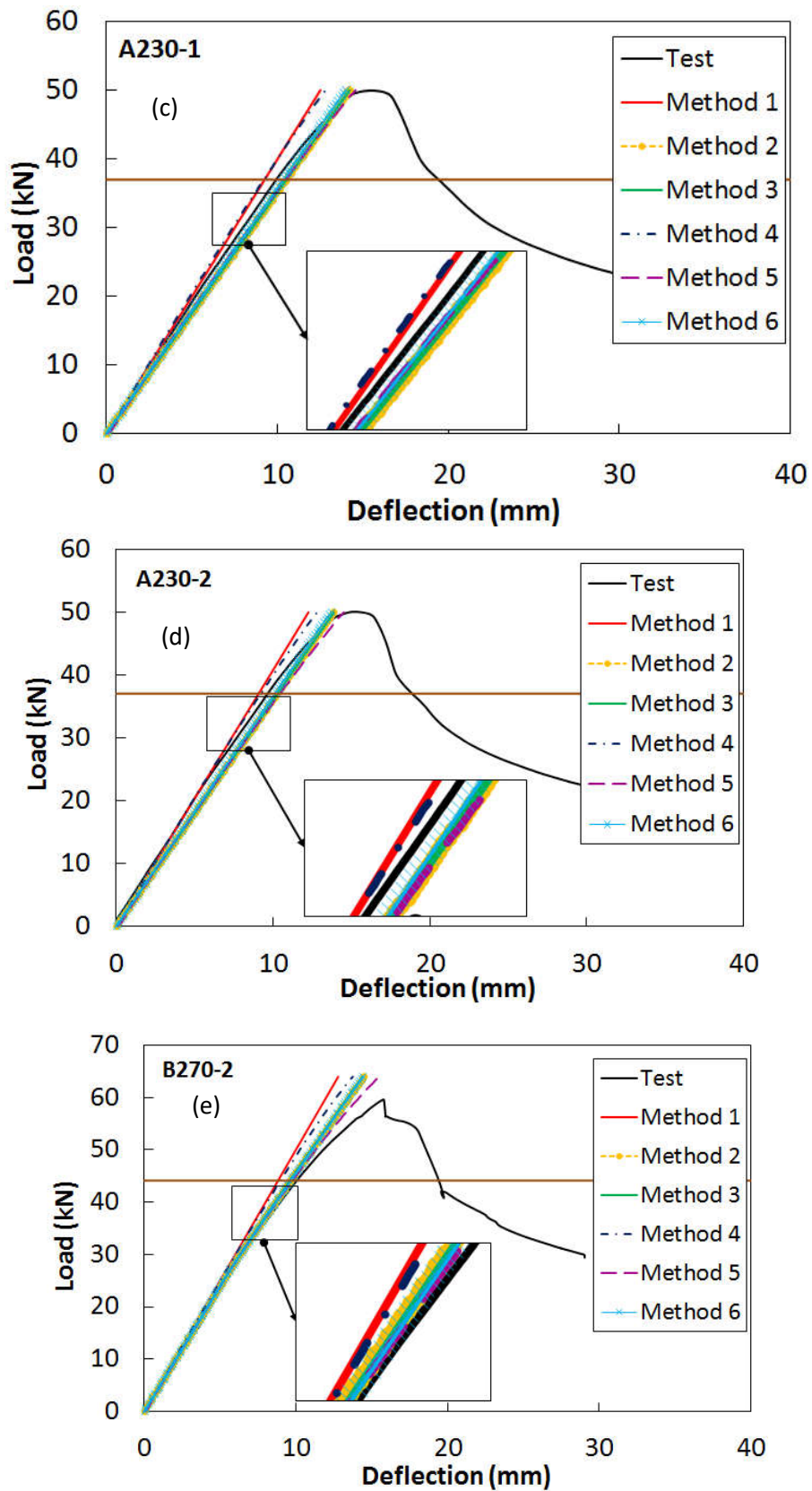


Figure 10: Load-deflection curves at mid span for the tested beams calculated using various methods and the physical test: specimens from (a)-(e)

A comparison between the calculated deflections using Methods 1 and 4, and similarly comparing Methods 3 and 5, shows that there is no significant difference between the results when the variation of secant modulus along the length of the beams is taken into account. This means that for the tested CFS beams, using the secant elastic modulus along the stress-strain curve have little effect on the determination of deflections, which agrees well with the EC3, Part 1-3, where no requirement is imposed on the secant modulus. The modulus of elasticity would be used for the design of the beams to serviceability limit state.

A comparison between the curves obtained from Methods 1 and 2 shows that the use of linear elastic properties for the cross-sections (i.e. full section properties) leads to underestimated deflections compared to the experimental results. The level of underestimation of deflection is 8% on average with a standard deviation of 2%, as shown in Table 3. When using reduced cross-sectional properties (I_{eff}) to calculate the deflections, Method 2 overestimates the deflections at the serviceability load. This is in line with the requirement of EC3, Part 1.3, where the effective cross-sections should be used in determination of the deflections.

A comparison between the results of Method 6 and the experimental measurements at the serviceability load shows that, in general, the EC3, Part 1-3 overestimates the deflections to a reasonable level, which can be acceptable in the practical design of CFS beams. It is also shown in Table 3 that the deflections of both standard and optimised beams were within the limit of $L/200=15.5\text{ mm}$, as recommended in [11]. Based on the average and also standard deviation of the errors, Method 6 (EC3 suggested method) provides the most accurate estimations of the beam deflections under serviceability loads.

Table 3: Comparison of the experimental and calculated deflections using various methods at serviceability load.

Specimens	Test	Method 1	Method 2	Method 3	Method 4	Method 5	Method 6	$\frac{\Delta_1}{\Delta_{test}}$	$\frac{\Delta_6}{\Delta_{test}}$
	Δ_{test} (mm)	Δ_1 (mm)	Δ_2 (mm)	Δ_3 (mm)	Δ_4 (mm)	Δ_5 (mm)	Δ_6 (mm)		
C180-1	10.4	9.7	11.5	11.5	9.4	11.1	11.2	0.93	1.08
C180-2	10.4	9.5	11.3	11.3	9.2	11.0	11.0	0.91	1.06
A230-1	9.9	9.2	10.5	10.5	9.1	10.4	10.3	0.93	1.04
A230-2	9.7	9.1	10.3	10.3	9.3	10.5	10.2	0.94	1.05
B270-2	9.9	8.9	9.7	9.7	9.0	9.9	9.7	0.90	0.98
Average								0.92	1.04
St. Dev.								0.02	0.04

6 EVALUATION OF THE OPTIMISATION PROCESS

In this section, the efficiency of the optimisation method briefly explained in Section 2 is further investigated. While section A230 is a standard commercially available cross-section, B270 is the optimised solution with highest flexural strength subject to constraints in Eq.(2)-(5) for a lipped channel beam. The nominal cross-sectional dimensions of these sections are given in Fig. 1.

Fig.11 compares the ultimate bending capacity of the standard and optimised sections for the CFS beams obtained from the experimental results, detailed FE models and EC3 design method. Based on the experimental results, it can be seen that the optimised shapes offer a much higher flexural strength (up to 19% higher) compared to the standard lipped channel section with the same amount of material. Similar results were obtained from FE models and EC3 design method, where the optimum design solutions showed around 20% higher flexural strength compared to the standard sections.

It should be mentioned that for the CFS beams (3100 *mm* span) used in this study, it was found that the serviceability constraints have been automatically satisfied within the optimisation process, as shown in Table 3. This has been confirmed by both the experimental and numerical results. The deflection of the optimised cross-section (Cross-section B) at the serviceability load level is around 10% less than that of the standard cross-section (Cross-section A). The reason is that the optimised beam cross-sections generally tend to be with a larger profile height, which leads to a larger stiffness with reduced deflections.

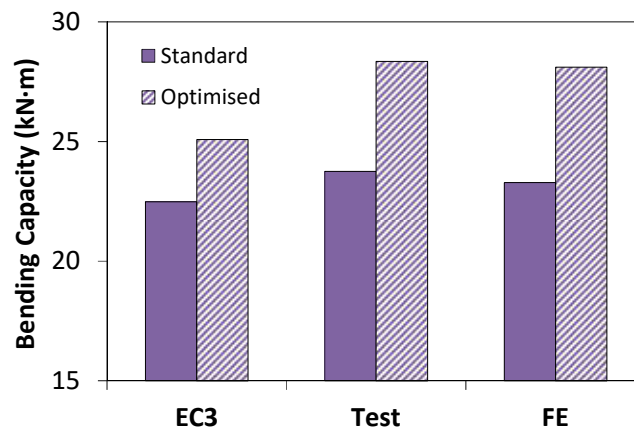


Figure 11: Flexural strength of the optimised and the standard sections using the same amount of material

It is worth noting that the trends of increasing/decreasing capacity and deflections over the range of sections for the CFS beams are very well predicted by EC3 when the tested results are taken as a benchmark. This indicates that the proposed optimisation method is reliable and can provide a practical tool for manufacturers and structural engineers to improve the capacity and stiffness of CFS beams.

The results of this study in general demonstrate the accuracy of the developed FE models to predict the flexural strength and deflections of CFS beams with different cross sectional shapes. These validated models should prove useful in practical applications for more efficient design of CFS back-to-back beams.

7 CONCLUSIONS

An advanced numerical model has been developed to study the local/distortional buckling behaviour and deflections of CFS lipped back-to-back channel beams and to verify the efficiency of a previously proposed optimisation framework. The model takes into account the non-linear stress–strain behaviour of CFS material, the strain hardening effects at the round

corners due to the cold-working process, and the experimentally measured initial geometric imperfections. The numerical model was validated against an experimental program on a total of 6 lipped channel back-to-back beams. The validated models were then used to assess the accuracy of EC3 and DSM design methods for standard and optimum design solutions. Based on the results presented in this paper, the following conclusions can be drawn:

(1) The ultimate capacity of the sections predicted by the FE models was on average less than 2% in variation from the experimental results. The proposed FE model was also successful in capturing the failure shapes and predicting the compressive strength of CFS columns subject to local and global buckling modes.

(2) It was shown that, in general, the geometric imperfections can change the FE predictions by up to 11%, while the strength variation caused by the strain hardening effect at the round corners has negligible effects (less than 5%) in general.

(3) Both DSM and EC3 resulted in accurate predictions of the beam flexural strengths. While DSM usually led to underestimated results, EC3 predictions were up to 10% overestimated with a standard deviation of 5% and 9%, respectively.

(4) Eurocode 3, Part 1-3 uses a reduced cross-sectional property to calculate deflections which slightly overestimates the deflections at serviceability load. However, using linear elastic full cross-sectional properties provides consistent underestimation of the deflections (8% on average).

(5) The bending capacity of the optimised CFS beams obtained from validated FE models and EC3 design methods were up to 20% higher than standard lipped channel sections with the same amount of material. The previously proposed optimisation framework leads to cross-sections with higher web height, thus increased stiffness. The results demonstrate the efficiency of the adopted optimisation method to improve the bending capacity and stiffness of CFS sections.

(6) The developed model takes into account the non-linear stress–strain behaviour of CFS material and the initial imperfection is able to provide verification on design optimisation of CFS beams. The strain hardening effects at the round corners due to the cold-working process can be ignored when improving the capacity and stiffness of CFS beams is the main objective.

ACKNOWLEDGMENTS

The authors would like to thank the EPSRC for their financial support for this work via the EPSRC grant EP/L019116/1.

REFERENCES

- [1] Fiorino L., Iuorio O. and Landolfo R., “Designing CFS structures: The new school bfs in naples”, *Thin-Walled Structures*, **78**, 37-47, 2014.
- [2] Lim J.B.P. and Nethercot D.A., “Ultimate strength of bolted moment-connections between cold-formed steel members”, *Thin-Walled Structures*, **41**, 1019-1039, 2003.
- [3] Lim J.B.P. and Nethercot D.A., “Finite element idealization of a cold-formed steel portal frame”, *Journal of Structure Engineering-ASCE*, **130**, 78-94, 2004.
- [4] Young B. and Yan J., “Finite element analysis and design of fixed-ended plain channel columns”, *Finite Element Analysis and Design*, **38**, 549-66, 2002.
- [5] ABAQUS. Version 6.7. Pawtucket, USA: Hibbitt, Karlsson & Sorensen, Inc, 2007.
- [6] CEN. *Eurocode 3: Design of Steel Structures, part 1-5: Plated structural elements*, Brussels: European Committee for Standardization, 2005.

- [7] CEN. *Eurocode 3: design of steel structures, part 1.3: general rules—supplementary rules for cold formed members and sheeting*, Brussels: European Committee for Standardization, 2005.
- [8] CEN. *Eurocode 3: Design of Steel Structures. Part 1-1: General Rules and Rules for Buildings*, Brussels: European Committee for Standardization, 2005.
- [9] Ma W.X., Becque J., Hajirasouliha I. and Ye J., “Cross-sectional optimization of cold-formed steel channels to Eurocode 3”, *Engineering Structures*, **101**, 641-651, 2015.
- [10] Ye J., Hajirasouliha I., Becque J. and Eslami A., “Optimum design of cold-formed steel beams using Particle Swarm Optimisation method”, *Journal of Constructional Steel Research*, **122**, 80-93, 2016.
- [11] Rhodes J., *Design of cold formed steel members*, Elsevier Applied Science, 1991.
- [12] Ye J., *More efficient cold-formed steel elements and bolted connections*, PhD thesis, The University of Sheffield, 2016.
- [13] Schafer B.W., Li Z. and Moen C.D., “Computational modeling of cold-formed steel”, *Thin-Walled Structures*, **48**, 752-762, 2010.
- [14] Haidarali M.R. and Nethercot D.A., “Finite element modelling of cold-formed steel beams under local buckling or combined local/distortional buckling”, *Thin-Walled Structures*, **49**, 1554-1562, 2011.
- [15] Wang L.P. and Young B., “Behavior of Cold-Formed Steel Built-Up Sections with Intermediate Stiffeners under Bending. I: Tests and Numerical Validation”, *Journal of Structural Engineering-ASCE*, **142(3)**, 04015150-1- 04015150-10, 2016.
- [16] Yu C. and Schafer B.W., “Simulation of cold-formed steel beams in local and distortional buckling with applications to the direct strength method”, *Journal of Constructional Steel Research*, **63**, 581-590, 2007.
- [17] Serror M.H., Hassan E.M. and Mourad S.A., “Experimental study on the rotation capacity of cold-formed steel beams”, *Journal of Constructional Steel Research*, **121**, 216-228, 2016.
- [18] Sabbagh A.B., Petkovski M., Pilakoutas K. and Mirghaderi R., “Experimental work on cold-formed steel elements for earthquake resilient moment frame buildings”, *Engineering Structures*, **42**, 371-386, 2012.
- [19] Sabbagh A.B., Petkovski M., Pilakoutas K. and Mirghaderi R., “Cyclic behaviour of bolted cold-formed steel moment connections: FE modelling including slip”, *Journal of Constructional Steel Research*, **80**:100-108, 2013.
- [20] Öztürk F. and Pul S., “Experimental and numerical study on a full scale apex connection of cold-formed steel portal frames”, *Thin-Walled Structures*, **94**, 79-88, 2015.
- [21] Gutierrez R., Loureiro A., Reinoso J.M. and Lopez M., “Numerical study of purlin joints with sleeve connections”, *Thin-Walled Structures*, **94**, 214-224, 2015.
- [22] Liu Q., Yang J. and Wang F.L., “Numerical simulation of sleeve connections for cold formed steel sigma sections”, *Engineering Structures*, **100**, 686-95, 2015.
- [23] Juvinall R.C. and Marshek K.M., *Fundamentals of machine component design*, John Wiley & Sons New York, 2006.
- [24] Bickford J.H., *An introduction to the design and analysis of bolted joints*, Marcel Dekker, New York, 1997.
- [25] Croccolo D., De Agostinis M. and Vincenzi N., “Failure analysis of bolted joints: Effect of friction coefficients in torque–preloading relationship”, *Engineering Failure Analysis*, **18**, 364-373, 2011.
- [26] Wong M.F. and Chung K.F., “Structural behaviour of bolted moment connections in cold-formed steel beam-column sub-frames”, *Journal of Constructional Steel Research*, **58**, 253-274, 2002.

- [27] Fisher J.W., *On the Behavior of Fasteners and Plates with Holes*, Fritz Engineering Laboratory, Department of Civil Engineering, Lehigh University, 1964.
- [28] Uang C.M., Sato A., Hong J.K. and Wood K., “Cyclic Testing and Modeling of Cold-Formed Steel Special Bolted Moment Frame Connections”, *Journal of Structural Engineering-ASCE*, **136**, 953-960, 2010.